Journal of Advanced Research 61 (2024) 151–164

Contents lists available at ScienceDirect

Journal of Advanced Research

journal homepage: www.elsevier.com/locate/jare

Original Article

Liver metastases across cancer types sharing tumor environment immunotolerance can impede immune response therapy and immune monitoring

Yuzhen Gao [a,g,1], Shipeng Chen [b,h,1], Hao Wang [c,1], Chenghao Wu [a,g], Rui An [a,g], Guoli Li [a,g], Min Yang [a,g], Ying Zhou [d], Yundong Zhou [e], Xinyou Xie [a,g], Hong Yu [f,*], Jun Zhang [a,g,*]

[a] Department of Clinical Laboratory, Sir Run Run Shaw Hospital of Zhejiang University School of Medicine, Hangzhou, Zhejiang, China
[b] Department of Laboratory Medicine, Xiamen Key Laboratory of Genetic Testing, The First Affiliated Hospital of Xiamen University, School of Medicine, Xiamen University, Xiamen, China
[c] Department of Gastroenterology, Ruijin Hospital Affiliated to Shanghai Jiao Tong University School of Medicine, Shanghai, China
[d] Department of Clinical Pharmacology, Key Laboratory of Clinical Cancer Pharmacology and Toxicology Research of Zhejiang Province, Affiliated Hangzhou First People's Hospital, Cancer Center, Zhejiang University School of Medicine, Hangzhou, China
[e] Shanghai Medical Innovation Fusion Biomedical Research Center, Shanghai, China
[f] Department of General Surgery, Sir Run Run Shaw Hospital, Zhejiang University School of Medicine, Hangzhou, Zhejiang, China
[g] Key Laboratory of Precision Medicine in Diagnosis and Monitoring Research of Zhejiang Province, Hangzhou, Zhejiang, China
[h] School of Clinical Medicine, Fujian Medical University, Fuzhou, China

HIGHLIGHTS

- The prognosis of patients with liver metastasis is worse than that of other metastatic cancers across cancer types.
- Part of patients with liver metastasis have common tumor environment immunotolerance.
- The immunotolerance with low immune cells expression contributed the main features of liver metastasis across cancer types.
- Liver metastasis common features score guides immunotherapy/ prognosis of liver metastasis, with KRT19 playing a key role.

GRAPHICAL ABSTRACT

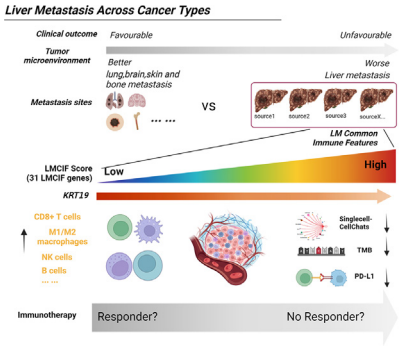

ARTICLE INFO

Article history:
Received 27 October 2022
Revised 16 July 2023
Accepted 19 August 2023
Available online 22 August 2023

Keywords:
Liver metastasis
Pan-cancer
Immunotolerance

ABSTRACT

Background: Hepatic immune tolerance might contribute to the development of therapeutic resistance to immunotherapy. However, addressing this issue is challenging since the efficacy of immunotherapy in the context of liver metastasis (LM) remains poorly studied. Here, we aimed to establish an LM common immune feature (LMCIF) score to quantify the characteristics of LM immunotolerance across cancer types for assisting clinical disease management.

Methods: Large-scale clinical data were collected to identify the prognosis of LM. Multi-omics datasets of metastatic cancers with LM special immune-related pathways (LMSIPs) from the Molecular Signatures Database (MSigDB) were used to obtain an LMCIF cluster. Based on differential expression genes (DEGs), a novel LMCIF score for the LMCIF cluster was constructed. In addition, multi-omics, and

* Corresponding authors at: Sir Run Run Shaw Hospital of Zhejiang University School of Medicine, Qingchun East Road, Jianggan District, Hangzhou 310016, Zhejiang, China (J. Zhang and H, Yu).
E-mail addresses: blueyu000@zju.edu.cn (H. Yu), jameszhang2000@zju.edu.cn (J. Zhang).
[1] Yuzhen Gao, Shipeng Chen and Hao Wang contributed equally to this work.

https://doi.org/10.1016/j.jare.2023.08.011
2090-1232/

Immunotherapy
KRT19

immunohistochemistry (IHC) data from the public and in-house cohorts were used to explore the features of LM, and LMCIF score.
Results: Patients with LM had a worse prognosis and significantly lower infiltration of immune cells than patients with metastasis to other organs when analyzed with combined clinical and RNA sequencing data. After extracting the LMCIF cluster from 373 samples by utilizing 29 LMSIPs and validating them in a microarray cohort, an LMCIF score was established to confirm the role of the immunosuppressive environment as a contributor to the poor prognosis of LM across cancer types. Moreover, this LMCIF score could be used to predict the immune response of cancer patients undergoing immunotherapy. Finally, we identified that the majority of the 31 LMCIF genes exhibited a negative correlation with TME cells in LM patients, one of them, KRT19, which possessed the strongest positive correlation with LMCIF score, was confirmed to have an immunosuppressive effect through IHC analysis.
Conclusions: Our results suggest that LM across cancer types share similar immunological profiles that induce immunotolerance and escape from immune monitoring. The novel LMCIF score represents a common liver metastasis immune cluster for predicting immunotherapy response, the results of which might benefit clinical disease management.

Introduction

Liver metastasis (LM), also known as secondary liver cancer, develops from cancers outside the liver, such as gastrointestinal tract tumors, lung tumors, breast tumors, and melanoma, and it occurs 18–40 times more frequently than primary liver cancers [1–2]. Metastatic liver cancers are increasingly common, resulting in a drastically lower 5-year survival rate and lower quality of life [3]. The complexity of the immune microenvironment complicates the treatment of liver metastases. Chemotherapy and radiotherapy, or either one in combination with multi-kinase inhibitors, such as sorafenib [4], regorafenib [5], or cabozantinib [6], have not shown significant clinical benefit so far, instead only the provision of short-term survival. The current approach to treating metastatic liver tumors involves immune checkpoint blockade that targets the immunosuppressive milieu [7–8].

The liver microenvironment is a complex cellular and molecular immune network, mainly including hepatic stellate cells (HSCs), liver sinusoidal endothelial cells (LSECs), Kupffer cells (KCs), regulatory T (Treg) cells, dendritic cells (DCs), and myeloid-derived suppressor cells (MDSCs) among others [2]. These resident liver cell subtypes play a key role in the mechanisms of hepatic immune tolerance. Among them, MDSCs are a heterogeneous population of bone marrow-derived cells that negatively regulate immune cell responses. Knolle PA et al. [9] have found that HSCs could promote the generation of MDSCs by secreting transforming growth factor-β (TGFβ) to form the tolerant immune orientation. KCs are liver tissue-resident macrophages, and they express programmed cell death ligand 1 (PD-L1) to mediate immunosuppressive orientation of the liver, and the depletion of KCs *in vivo* can abolish hepatic tolerance [10]. In addition, the polarized state of KCs could reduce the expression of major histocompatibility complex (MHC) on LSECs to limit immunostimulation [11]. Treg cells impair tumor-cytotoxic T cells by expressing CD25 and cytotoxic T lymphocyte protein 4 (CTLA4), as well as secreting several cytokines that promote the immunosuppressive microenvironment, such as TGFβ and IL-10 [12,13]. Pacella I et al. [14] have proved that the expansion of Treg cells significantly impairs the antitumor activity of tumor-cytotoxic T cells through increased utilization of lipids and glucose. Hepatic DCs includes two main subtypes: conventional DCs and plasmacytoid-derived DCs, respectively. Plasmacytoid-derived DCs respond poorly to toll-like-receptor (TLR) stimulation, and they can decrease the expression of costimulatory molecules, thereby contributing to the immunotolerance of the live [15]. All of the above hepatic immune tolerance mechanisms may, in turn, drive therapeutic resistance to immunotherapy [16]. However, the molecular features that underlie the mechanisms of human hepatic immunotolerance lead to compromised efficacy of immunotherapy remains to be elucidated.

Therefore, in the current study, we systematically analyzed overall survival in metastatic patients, with or without immunotherapy, across various cancer types and observed that patients with LM manifest the worst outcomes. Furthermore, we found hepatic immune microenvironment characteristics differ from those of other metastatic organs through the analysis of immune pathway-related genes. We then constructed a liver metastasis common immune feature (LMCIF) score representing the immunosuppressive microenvironment, which would, in turn, can be a predictor of immunotherapeutic efficacy for patients with LM. Finally, a representative hub gene, KRT19 was observed, and IHC experiments confirmed the negative correlation between KRT19 and infiltrating $CD8^+$ T cells. Our LMCIF score helps quantify the distinct immunosuppressive microenvironment of liver metastases, and it provides an effective prediction of prognosis and immunotherapy response in patients with liver metastases across cancer types.

Materials and methods

Study design and data collection

The experimental design we employed was illustrated in Fig. 1, which can be divided into the following sequential steps. First, to systematically identify the prognosis and tumor microenvironment (TME) of LM across cancer types, one study included 25,000 patients with metastasis and detailed prognosis information [17]. In addition, Dan R. Robinson et al. performed RNA sequencing across different cancer types, of which>500 cancer metastasis patients were also collected [18]. Among them, the total of 373 metastasis samples with RNA transcripts, containing liver (n = 212), lung (n = 59), brain (n = 9), bone (n = 67), and skin (n = 26), were directly extracted from the RNA transcripts matrix in the MET500 cohort by deleting the original local metastasis samples [18]. Single sample gene set enrichment analysis (ssGSEA) was utilized to quantify cells within the TME and to discriminate the TME of LM from metastases derived from other organs.

In the next step, we used the **373** metastasis samples from more than 16 cancer types, and 2432 normal tissue samples from the above 5 organ sites to perfrom further analysis. A total of 2432 normal samples with RNA transcripts, which including the 110 normal liver tissues and other tissues (Brain (n = 1152), Bone (n = 70), Skin (n = 812), and Lung (n = 288)), were selected from the GTEx database(https://www.gtexportal.org/home). Based on RNA

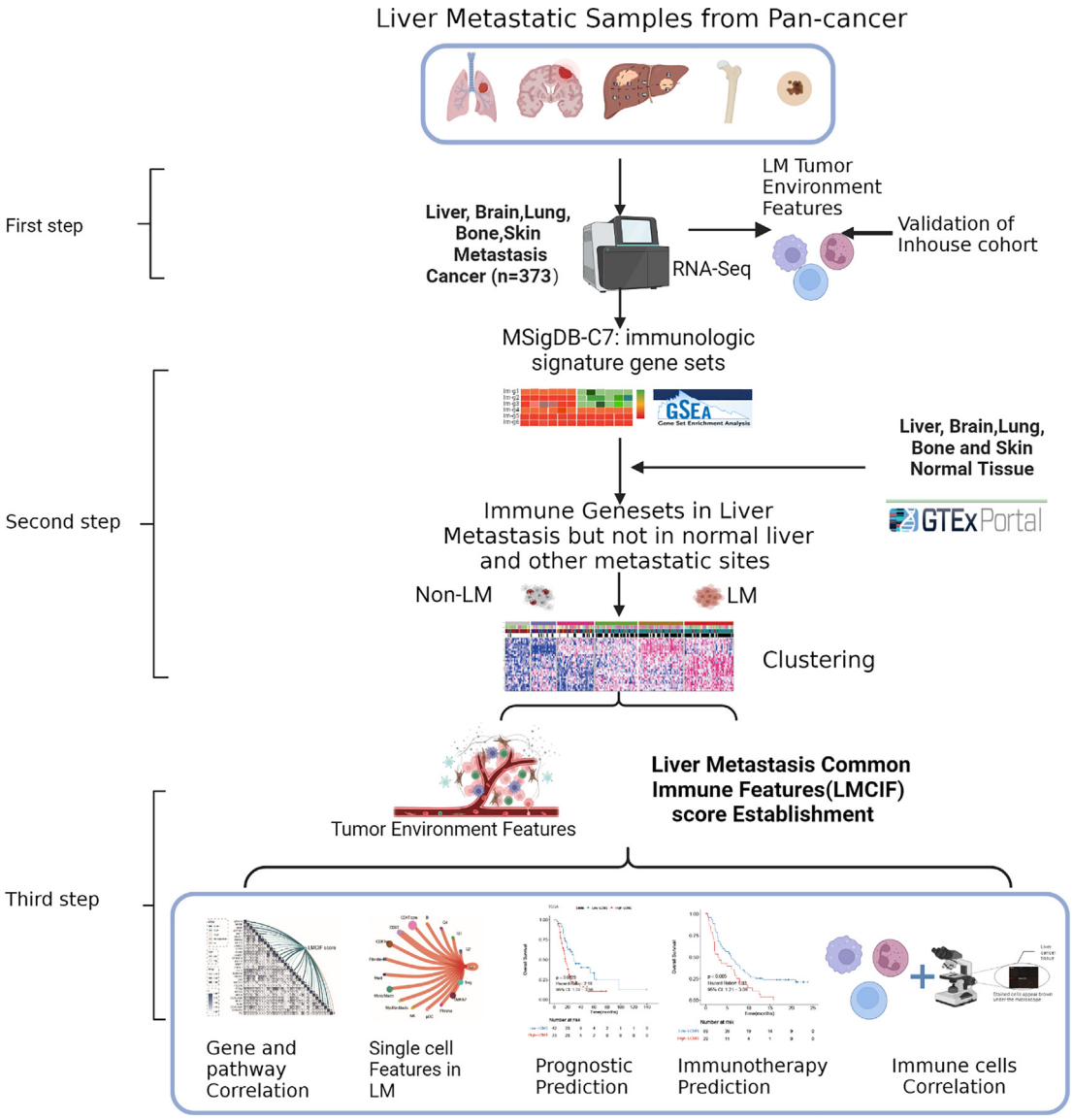

Fig. 1. Overall design of this study. First step: Clinical analysis for Liver metastasis(LM). We used the 25,000 patients with pan-cancer and OS data to check the porpartions and the prognosisitc values of LM. Then, 301 pan-cancer with Immunotherapy was matched to detected the Immuntoherapy effect for LM. Second Step, Clusting analysis. After estimating the TME charactertics of LM, by using the 5000 + MSigDB-C7 pathways, 373 patients with RNA-sequence data were clustering. Third Step: LMCIF score establishing and estimation. The TME features and find special genes of LMCIF clusters were identified to construct the LMCIF score. In-house and extral data were used to validate the role of related genes in the LMCIF score. The drawing was produced by BioRender (https://biorender.com/).

transcripts, the enrichment scores of 5025 immune pathways from MSigDb C7 (https://www.gsea-msigdb.org/gsea/msigdb/index.jsp) in all metastatic cancer patients and normal tissues were calculated, respectively. Subsequently, LM samples with special differential expression immune-related pathways (LMSIPs) were identified to cluster them. These LM special clusters were now termed as LMCIF clusters and the features of LMCIF clusters were further characterized.

In the end, an LMCIF score based on the different expressing genes in LM was developed. It represents the genetic traits or phenotypes associated with LMCIF clusters in LM patients [18], LM patients undergoing immunotherapy [19–20] and LM single cells [21]. Also, the tissue samples from colorectal cancer associated with LM as in-house data, as well as a public dataset (GSE51244), were both used to validate the characteristics of LMCIF-related genes. All datasets utilized in the present work were listed in **Supplemental Table S1**.

Prognostic analysis of LM in pan-cancers with or without immunotherapy

A total of 10,097 metastasis patients out of 25,000 patients across cancer types were included in the prognostic analysis of LM [17]. Kaplan-Meier (KM) curves and Cox proportional hazards regression analysis were used to reveal the role of LM for tumor progression in different cancer type. A cohort of 301 metastasis patients who received immunotherapy, extracted from a larger group of 2,277 patients [20], was utilized to assess the prognosis of LM.

Quantifying TME cells, immune pathways, and immune scores

By using various bioinformatics tools, such as digital quantitative or non-quantitative methods, the gene expression data of immune cells, stromal cells, and other important components

within the TME from all avivalbe metastasis samples were interrogated based on the RNA transcripts. For TME cells, the gene signature-based method xCell [22–23] and MCP-counter (Microenvironment Cell Populations-counter) [24] were adopted to integrate the advantages of gene set enrichment with deconvolution approaches. In addition, both immune and environment scores were measured by the xCell algorithm. The estimate R package was used to measure stromal score, immune score, and estimate score [25–26]. Classical canonical pathways and immunotherapy-predicted response-related pathways, which had been selected manually from previous studies, were listed in **Supplemental Table S2**. These essential pathways were also calculated by gene set variation analysis (GSVA) to explore cancer progression and immune features of LM in the present study. To reveal the full immune landscape of LM patients across cancer types, the immune features of 5025 immune-related gene sets from MsigDB were also calculated via ssGSEA methods. All obtained calculated scores and Z-scores were analyzed according to scale for further analysis.

Identification of LM special immune-related pathways

To find LM special immune-related pathways (LMSIPs), GETx database and pan-cancer cohorts were used. Then, we used the lmFit function of the "limma" package to identify the target immune gene sets from a total of 5025 genes more highly expressed in liver metastasis samples compared to other tissue samples in the pan-cancer cohort. Lastly, we kept the immune gene sets with significantly high expression in LM samples and excluded those with significantly elevated expression in normal liver tissue (T value > 6 and p adj < 0.001) in further analysis of LM samples.

Immune clustering for metastatic cancer

Given these LMSIPs, we performed a non-parametric unsupervised analysis to estimate the variation of these metastasis samples. First, sample distances were computed by the "dist" function in R with Euclidean distance, followed by generating clusters for distances by the "Ward-D2" linkage method by the "hclust" function. In addition, through the "cutree" function, we established clusters to include specific samples. Finally, for visualization purposes, heatmaps and boxplots were performed with a representation of 373 samples and LMSIPs.

Validation of immune clustering in the Gene Expression Omnibus (GEO) dataset

To verify the immune genetic profile of metastasis clustering, we searched special cohorts with metastatic cancer in the GEO dataset (https://www.ncbi.nlm.nih.gov/geo/). A total of 374 metastasis samples from 16 datasets from a previous study were collected. Data were downloaded from https://github.com/odap-ubs/mets-immunecluster. GSVA calculates sample-wise gene set enrichment scores as a function of genes inside and outside the gene set, analogously to a competitive gene set test. By using the GSVA score for the above LMSIPs, we then clustered the metastasis samples to get their genetic profile. Other characteristics, including some TME cells and special pathways, were also identified for further analysis in each immune cluster of metastasis samples.

Identification and development of LMCIF score

To better understand the role(s) of LMCIF clusters in LM, we aimed to establish a score representing the biological significance of LMCIF. To accomplish this, RNA transcripts between clusters with the highest proportion of LM, and clusters with the lowest percentage of LM were compared. Their DEGs were identified as LMCIF genes (logFC > 1.5, adjusted P < 0.001). Among these LMCIF DEGs, we excluded the highly-expressing genes in the normal liver tissue samples from GTEx as well (logFC > 1.5, adjusted P < 0.001). Given the significant DEGs in LM, principal component analysis (PCA) was used to establish the LMCIF score in all samples. Similar to a previous study [27], we summed the principal components PC1, PC2 and PC3 as the LMCIF score. The Z-score was applied to the LMCIF score and used in the present study to indicate how much a given value differs from the standard deviation.

$$\text{LMCIF Score} = \sum_{i}^{j}(PC1i + PC2i + PC3i)$$

Where i is the array or gene sequence expression of LMCIF genes, and j is the total number of DEGs in the LMCIF cluster.

Function enrichment analysis

Gene Ontology (GO) terms and Kyoto Encyclopedia of Genes and Genomes (KEGG) pathway analyses for DEGs were performed by the "clusterProfiler" package and visualized by the network function in R.

Cell-cell communications in LM single-cell data

Single-cell data were obtained from the GEO (GSE178318). Among them, 54,305 single cells were identified from the liver metastasis tissues of colon cancer. First, the maestro pipeline was used to annotate all single cells in CD4Tconv, B, CD8T, CD8Tex, Fibroblasts, Mast, Mono/Macro, Myofibroblasts, NK, pDC, Plasma, TMKI67, Treg and Cancer cells. The tSNE function from the Seurat R package was used to visualize LM single cells. Then, based on DEGs, we first used AddModuleScore in Seurat R for cancer cells. Next, to check the different effects of cancer cells with different LMCIF scores on other TME cells, cancer cells were divided into four zones, Q1, Q2, Q3 and Q4, according to quantity. CellChat is an R package containing ligand-receptor interactions. It can analyze the intercellular communication from scRNA-seq data, and it was used to evaluate the major signaling inputs and outputs among all TME cell clusters, using CellChatDB.human. Finally, the "netVisual_circle function" was used to show the strength or weakness of cell–cell communication networks from the target cell cluster to different cell clusters in all clusters.

The utilization of the LMCIF score as a predictor of prognosis and immunotherapy in patient cohorts

To test the prognostic value of the LMCIF score in pan-cancer, we collected 115 patients with LM from 13 cancer types in the TCGA cohort. In addition, patients with immunotherapy (n = 348) were taken from the "IMvigor210" R package. These LM patients had advanced urothelial cancer and had been administered atezolizumab, an anti-PD-L1 antibody. They were included to explore the relationship between the LMCIF score and immune checkpoint blockade (ICB) therapy response in patients with LM.

Ethics statement

The use of all human samples was approved by the Institutional Ethics Committee of the Sir Run Run Shaw Hospital of Zhejiang University School of Medicine (Ethical code: 20190211–55). Informed consent was obtained from all patients.

Human sample collecting and immunohistochemical staining

We made a tissue microarray [No.XM091Mco1] with 14 pan-cancer metastatic samples, which cooperated with Xi'an Biotech Co., Ltd (Xi'an, China). All tissue samples were fixed in formalin and embedded with paraffin. Multiplexed Immunohistochemical Staining was supported by Baios Biotechnology Co., Ltd. KRT19 Polyclonal Antibody (PTG,60187–1-AP) and CD8 antibody (ZA-0508) was purchased from Zhongshan Golden Bridge and recovered by PH9.0 EDTA. Secondary antibodies of Alexa Fluor®488 Donkey anti- Rabbit (A21206) and Alexa Fluor®594 Donkey anti-Mouse (A21203) were purchased from Life Technologies.

For double-IHC, the following steps were adopted. First, after deparaffinization, rehydration, and antigen retrieval, the tissue microarray was placed in TBST and blocked with 10% Donkey Serum for 30 mins at room temperature. In addition, after incubating 0.5 μL mouse monoclonal anti-human CK19 antibody (EDTA, dilution 1:2000) and 1 μL rabbit monoclonal anti-human CD8 (EDTA, dilution 1:1000) in the microarray overnight at 4 ℃, the working solution of secondary antibodies was used for configuration the next day, and slides were incubated at 37 ℃ for 60 mins. DAPI (1:500) was then used to stain nuclei for 5 mins while kept away from light. Diaminobenzidine (DAB) Substrate Kit was used for the chromogenic reaction. Finally, IHC images were captured by the digital slide scanning system (3DHistech). Green represented the positivity of CD8, and red indicated the positivity of KRT19.

Immunohistochemical score

To detect the immunohistochemical score (H-score) and the density of positive and negative cells in each sample, two experienced pathologists with artificial intelligence (AI) tools (Visiopharm, OpenSlide and Python) extracted these features from cancer tissue samples. Here, H-score is a histological scoring method for processing immunohistochemical results. It converts the number of positive cells and their staining intensity in each section into corresponding values for semi-quantitative staining of tissues. Following the equation H-score = Σ Pi (i + 1), Pi represents the percentage of the positive cells in all cells in a section, and i represent staining intensity. The immunohistochemical H-score integration method was [1 × (proportion of cells with a staining score of 1) + 2 × (proportion of cells with a staining score of 2) + 3 × (proportion of cells with staining score of 3)] [28]. All available features could be extracted from the AI results, including the number of negative and positive cells, the positive percentage, and the number of positive cells per mm^2 for each sample.

Statistical analysis

The categorical variables were presented as frequencies and percentages in tables or bar plots and compared for significance using the chi-square test. The continuous variables were reported as median values with interquartile ranges (IQR) or mean values ± standard deviation (SD) based on normality in the tables or the box plots. The non-normally distributed continuous variables were compared for significance using the Wilcoxon rank-sum test between two groups and the Kruskal-Wallis H test for more than two groups. Additionally, the log-rank (Mantel-Cox) test and univariate Cox proportional hazards regression were used to analyze the prognosis of variables in patients with LM, with or without immunotherapy. The Spearman method was employed to calculate the relationships between two continuous variables with non-normal distribution. The statistical parameters, including the definition of center, dispersion, precision measures, and statistical significance, were reported in the figures and figure legends. Any other special analyses can be found in the description of the corresponding method sections. All statistical analyses were conducted using R 3.6.2. A p-value of < 0.05 was considered statistically significant.

Results

High incidence and poorer prognosis of LM in pan-cancer with or without immunotherapy

According to the statistics of clinical data from 25,000 patients, 10,097 patients from 27 cancer types were identified had cancer metastasis (with or without LM) and were included in the initial stage of analysis. LM accounted for 4.8% to 62.7% of pan-cancer types (Fig. 2**A and Supplemental Table S2**). Among them, gastrointestinal and neuroendocrine tumors, pancreatic and colorectal cancer, showed the highest incidence of LM. In addition, Cox regression analysis was performed and revealed that LM had a significant negative effect on survival in almost all cancer types (Fig. 2**B, Supplemental Table S2, and Figure S1**). Especially, germ cell tumor, cervical cancer, and thyroid cancer demonstrated higher Hazard Ratio(HR) values of LM for the prognosis. Survival curves showed that LM is a significant risk factor in several typical solid tumors, such as melanoma, bladder, lung, ovarian, breast, and colorectal (Supplemental **Figure S1**). Based on all datasets, it was clear that cancer patients accompanied by LM had a poorer prognosis than those who had other organ metastases in pan-cancers (Fig. 2**C, P < 0.001**). Furthermore, 401 patients with anti-PD-1/PD-L1 treatment across 8 different cancer types were enrolled to evaluate the influence of LM on prognosis (Supplemental **Table S3**). Under anti-PD-1/PD-L1 immunotherapy, LM patients still had worse outcomes than non-LM patients (Fig. 2**D, P < 0.001**). Collectively, the results indicated that patients with LM tend to have poorer prognosis than those who have other organ metastases.

Tumor microenvironment (TME) of LM across cancer types

To investigate the TME of LM, various TME profile indicators, including tumor mutation burden (TMB), immune score and infiltration of B cells and T cells, were calculated by using DNA mutation or RNA-seq data. Interestingly, it was found that TMB, an immune indicator for immunotherapy, was significantly lower in patients with LM than those without LM with and without immunotherapy (Fig. 2**E and 2F**). Next, by the MCP-counter, we found that most immune lineages were lower in patients with LM compared to those without LM metastasis, including B lineages, NK cells, monocyclic lineage, myeloid dendritic cells, T cells and in particular CD8 T cells (Fig. 2**G, all P < 0.05**). Similarly, for samples with Estimated and xCell algorithm for pan-cancer RNA transcripts, immune score, stromal score, estimated score, microenvironment score, as well as 64 types of immune cells were calculated. And the results revealed that these immune indicators were all significantly lower in patients with LM compared to those without LM (Fig. 2**H and** Supplemental **Figure S2**).

To further validate this observation, we conducted an immunohistochemical assay to assess the expression of CD8 protein in 25 samples from 4 types of cancer metastasis (e.g., liver, lung, bone, and brain) on a tissue chip, representing pan-cancer metastasis samples. The result further validates that the tumor-infiltrated number of $CD8^+$ T cells was significantly lower in the LM tissue than in non-LM tissue (e.g., lung, brain and bone) (Fig. 2**J, P < 0.05**). Fig. 2**I** displays a representative sample exhibiting low levels of $CD8^+$ protein in LM tissue, while another representative sample shows high levels of $CD8^+$ protein in the non-LM tissue.

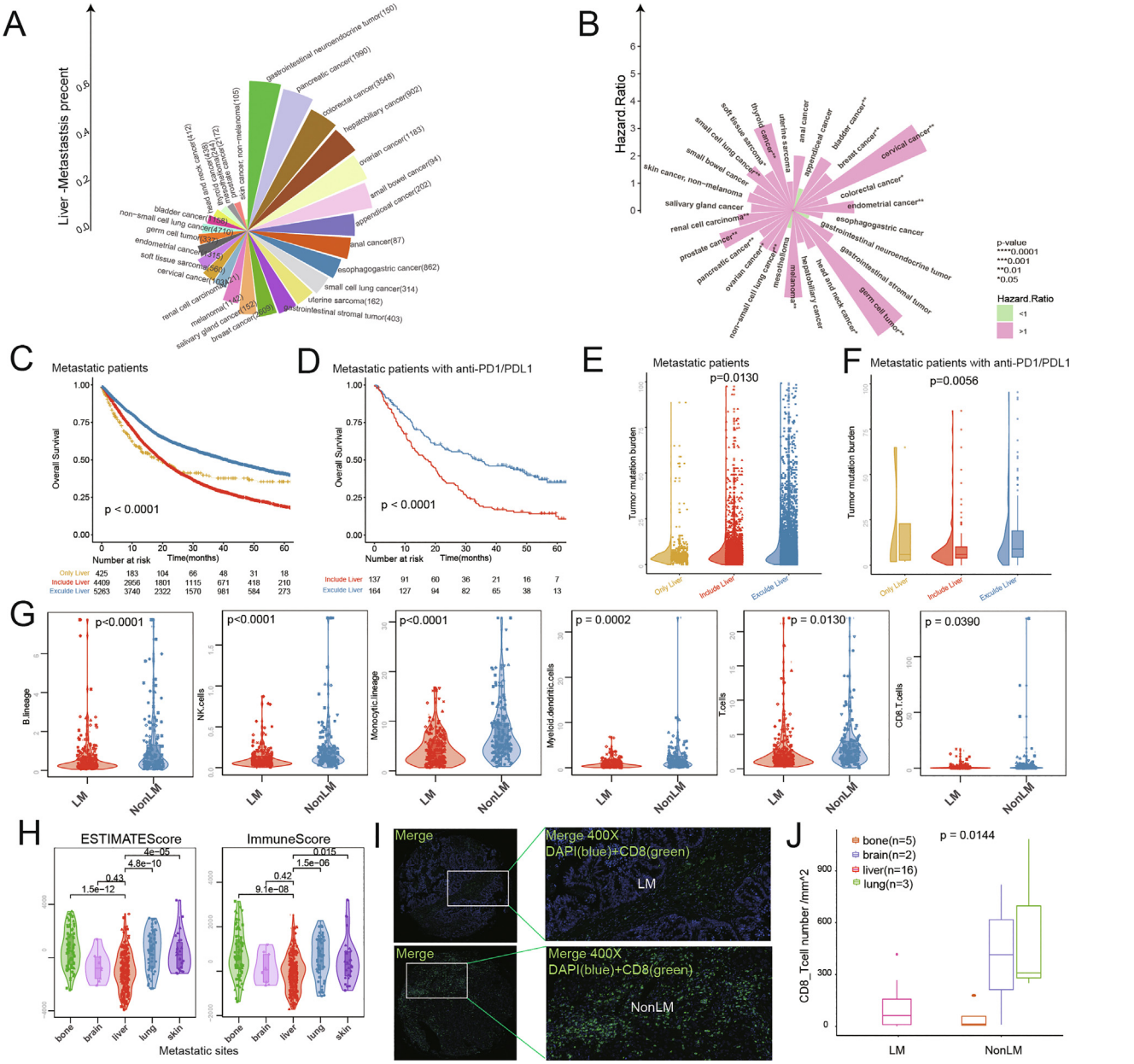

Fig. 2. LM shares a poor prognosis and a similar immune environment. A) Rank of incidence of LM in each cancer type. B) Cox regression for the prognosis ranks for LM in each cancer type. C) and D) Log-rank test for the KM curves in the *meta*-cohort of metastasis patients with or without anti-PD1/PDL1 immunotherapy. E) and F) Kruskal-Wallis test for the TMB in different statuses of LM with or without immunotherapy. G) Wilcoxon test for the different infiltration of immune cells in metastasis cancer patients with or without liver metastasis. H) Kruskal-Wallis test for the different TME scores five types of metastases from the patients with 16 cancer types. I) IHC for CD8 protein in the representative samples from LM or non-LM tissue. J) Kruskal-Wallis test for the expression of CD8 T cell number among four organ metastases.

All these continus data were presented with correspondence format in the Supplemental **Table S4**. In summary, compared to metastases in other organs, LM showed significantly lower immune cell infiltration.

Clustering for metastatic cancers based on LM special immune-related pathways (LMSIPs)

We then hypothesized whether there are certain common immune chrematistics in patients with LM. To test this hypothesis, precise extraction of genetic features for patients with LM was achieved by using the criterion of limma t value > 6 and adjusted p-value < 0.001, both in LM samples and normal liver samples (Fig. 3**A and 3B**). This yielded 29 LMSIPs with their statistic information for LM (Fig. 3**C,** Supplemental **Table S5, and Table S6**). Next, in the 373 metastasis samples, cluster analysis was performed according to the GSVA score of 29 LMSIPs. Six immune metastasis clusters with obvious differences in the expression of LMSIPs were discovered(Supplemental **Figure S3 and Table S7**). A positive relationship between the expression of 29 LMSIPs and the percentage of LM was observed (Fig. 3**D**). Among these immune clusters, cluster 4 had the highest proportion of LM (Fig. 3**E**). The bar plot also showed that the distribution of these clusters was significantly different in 16 primary cancer types (Fig. 3**F**).

Characteristics and validation of special liver metastasis clusters

In addition, to explore the characteristics of different LMCIF clusters, several immune features and tumor-activated pathways were calculated by GSVA in the 373 metastasis samples (Fig. 4**A**).

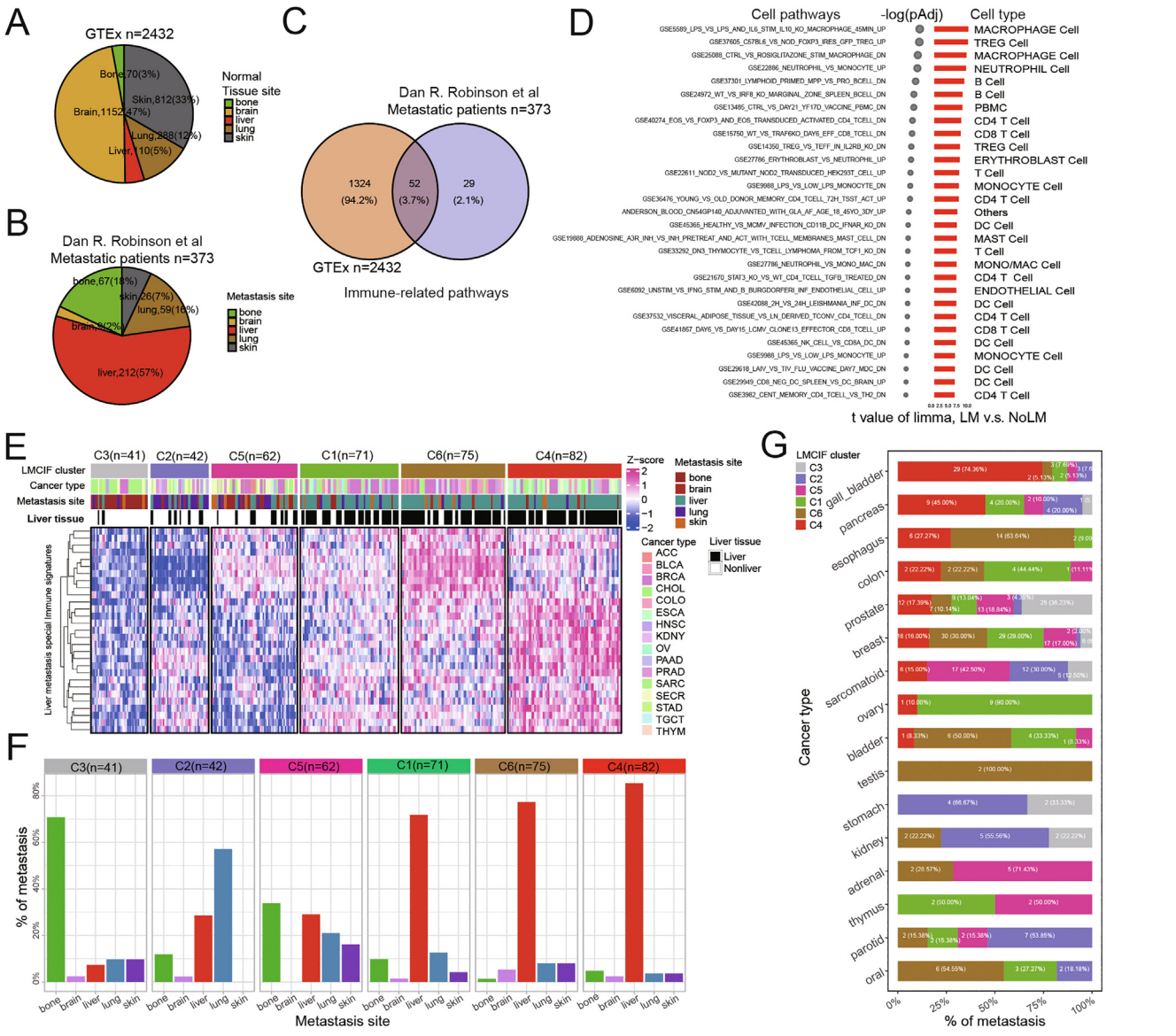

Fig. 3. Clustering analysis for LMCIF patients using immune pathways. A) Proportion of liver source in the normal issue from GTEx(n = 2432). B) Proportion of liver source from metaststic patients(n = 373). C) Venn plot of crossing selection for the targeting LMSIPs in the LM cluster C4. D) Limma results for the LMSIPs with immune cell source by cross selection. E) Six LM clusters by using 29 LMSIPs in metastasis samples. F) Bar plot of proportation of the six clusters in each metastasis cancer type. G) Precentage of the different distribution of six LM clusters in original each cancer type. Abbreviation: ACC Adrenal; BLCA Bladder; BRCA Breast; CHOL Gall bladder; COLO Colon; ESCA Esophagus; HCC Liver; HNSC Head-neck; KDNY Kidney; OV Ovarian; PAAD Pancreas; PRAD Prostate; SARC Sarcoma; SECR Miscellaneous gland; STAD Stomach; TGCT Germ-cell; THYM Thymoma.

Of note, clusters with high LM proportion had the fewest immune cell infiltrations and the most suppression of immune response. For example, cluster C4, which showed the highest LM percentage, showed lower infiltration of the lymphoid and myeloid cells, while some stromal cells were highly infiltrated (Fig. 4**A**). To further validate the genetic profiles of LM, a combined dataset, including 374 samples with four different metastasis sites (bone, brain, liver, and lung), was included and termed the *meta*-GEO cohort (Supplemental **Table S8**). The 29 LMSIPs were also used to cluster these samples. We observed that one of the LMCIF clusters had the lowest number of immune cells and a higher number of suppressed immune response pathways. Additionally, this cluster exhibited the highest rates of LM compared to the other clusters in the *meta*-GEO corhot (Fig. 4**B,** Supplemental **Figure S4 and** Supplemental **Table S8**). All genesets compared among these immune clusters were listed in Supplemental **Table S9.** These continus data in the heatmap were presented with correspondence format in the Supplemental **TableS10**.

Development of LMCIF score for LM patients

To better reveal the characteristics of LMCIF, 305 of its differential expression genes (DEGs) between clusters with the highest and lowest LM rates (C4 *vs.* C3) from the RNA-seq data of 373 metastasis cohorts were identified. We also delimited 274 background DEGs derived from normal liver tissue and other normal tissues in the GTEx database. The special liver genes were obtained (Supplemental **Table S11**). Finally, 31 DEGs were deemed LMCIF genes that might represent the features of LMCIF C4 cluster in the metastasis samples (Fig. 5**A 5B, 5C, and** Supplemental **Table S12**). GO terms analysis for these 31 DEGs showed that their most associated functions include cell-substrate adhesion, cornification, and

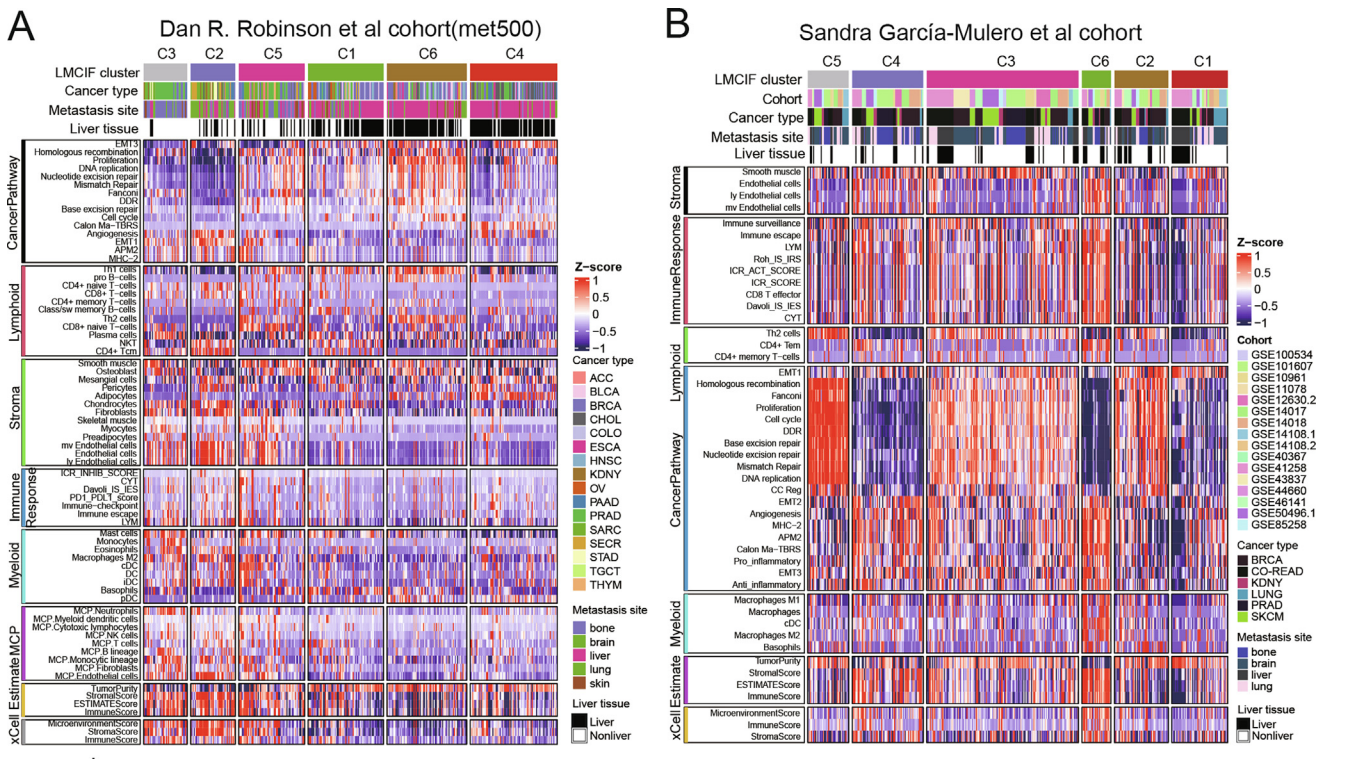

Fig. 4. Heatmap of the comparison of cancer gene signatures, immune response signatures and TME cells among different LMCIF clusters. A) Training cohort (Dan R. Robinson et al. cohort) B) Validation cohort (Sandra García-Mulero et al. cohort). All variables with $p < 0.001$ was tested by Kruskal.test among six groups. Abbreviation: ACC Adrenal; BLCA Bladder; BRCA Breast; CHOL Gall bladder; COLO Colon; ESCA Esophagus; HCC Liver; HNSC Head-neck; KDNY Kidney; OV Ovarian; PAAD Pancreas; PRAD Prostate; SARC Sarcoma; SECR Miscellaneous gland; STAD Stomach; TGCT Germ-cell; THYM Thymoma.

epidermal cell differentiation. All of these functions are important factors involved in the metastatic process (Fig. 5**D**). We then performed a prognosis analysis for these 31 LMCIF genes on the GEPIA (Gene Expression Profiling Interactive Analysis) website and found most of them are significantly related to poor prognosis in pan-cancer (Supplemental **Figure S5**). Moreover, we developed an LMCIF score for metastasis samples by using the 31 DEGs and their coefficients (Supplemental **Table S13**). Association analysis revealed that the LMCIF score was strongly related to LMCIF genes (Fig. 5**E**).

Liver organ specificity of LMCIF score

To explore the liver organ specificity of the LMCIF score, we first observed that the LMCIF score was higher in the LMCIF C4 than in other metastasis immune clusters except for C1 and C6 (Fig. 5**F**). Then, we compared the LMCIF score in different metastasis tissues and found that the LMCIF score was higher in LM than in bone and lung metastasis, while no significant differences between brain and skin metastasis were detected (Fig. 5**G**). Interestingly, the LMCIF score had no significant differences among breast, esophagus, gallbladder, or prostate cancer with metastasis (all cancer samples $n > 20$) (Fig. 5**H**). The LMCIF score with statsitc information for each group were listed in the Supplemental Table 14.

LMCIF score indicates a suppressed immune microenvironment

In metastasis samples, LMCIF score was found to be negatively correlated with immune cells, including myeloid dendritic cells, NK cells, T cells, as well as B and monocytic lineage cells (Fig. 6**A and** Supplemental **Figure S6**). In addition, in the single-cell analysis, all LMCIF genes were highly expressed in tumor cells (Fig. 6**B**). Next, by using quantile values of LMCIF genes, single LM tumor cells were labeled with the single-cell LMCIF score ($n = 5527$), and it was noted that tumor cells had a much higher LMCIF score than other cells at the single-cell resolution (Fig. 6**C**). Then the tumor cells were divided into four subgroups based on LMCIF scores (from low to high: Q1, Q2, Q3, and Q4). CellChat analysis indicated that immune cells showed reduced crosstalk with single cancer cells along with an increase in LMCIF score (Fig. 6**D and** Supplemental Table 15).

LMCIF score predicts unfavorable prognosis and limited immunotherapy response

To study the effect of LMCIF on prognosis and immunotherapy response, we integrated 115 pan-cancer patients with LM in the TCGA cohort and observed that a higher LMCIF score correlated with a worse prognosis in these tumors (Fig. 6**E and** Supplemental **Table S16**). In addition, LMCIF score of all metastasis sites showed predictive value for patients' prognosis under anti-PD-L1 immunotherapy (Fig. 6**F**). Among them, 98 patients identified as LM patients were used to validate the prognostic value of the LMCIF score (Fig. 6**G**). These patients, along with their LMCIF scores, were listed in Supplemental **Table S17**.

Validation of representative genes of the LMCIF score

We firstly detected the correlation of 31 LMCIF genes with TME cells in the LM patients, and found that most of them were negatively related to Immune cells(Fig. 7A). Amongt them, KRT19 was identified as one of the representative genes consisting of LMCIF score, since it had the highest relationship with the LMCIF score in metastatic cancers ($R = 0.94$, $P < 0.001$, Fig. 5**E**). Multiplex IHC

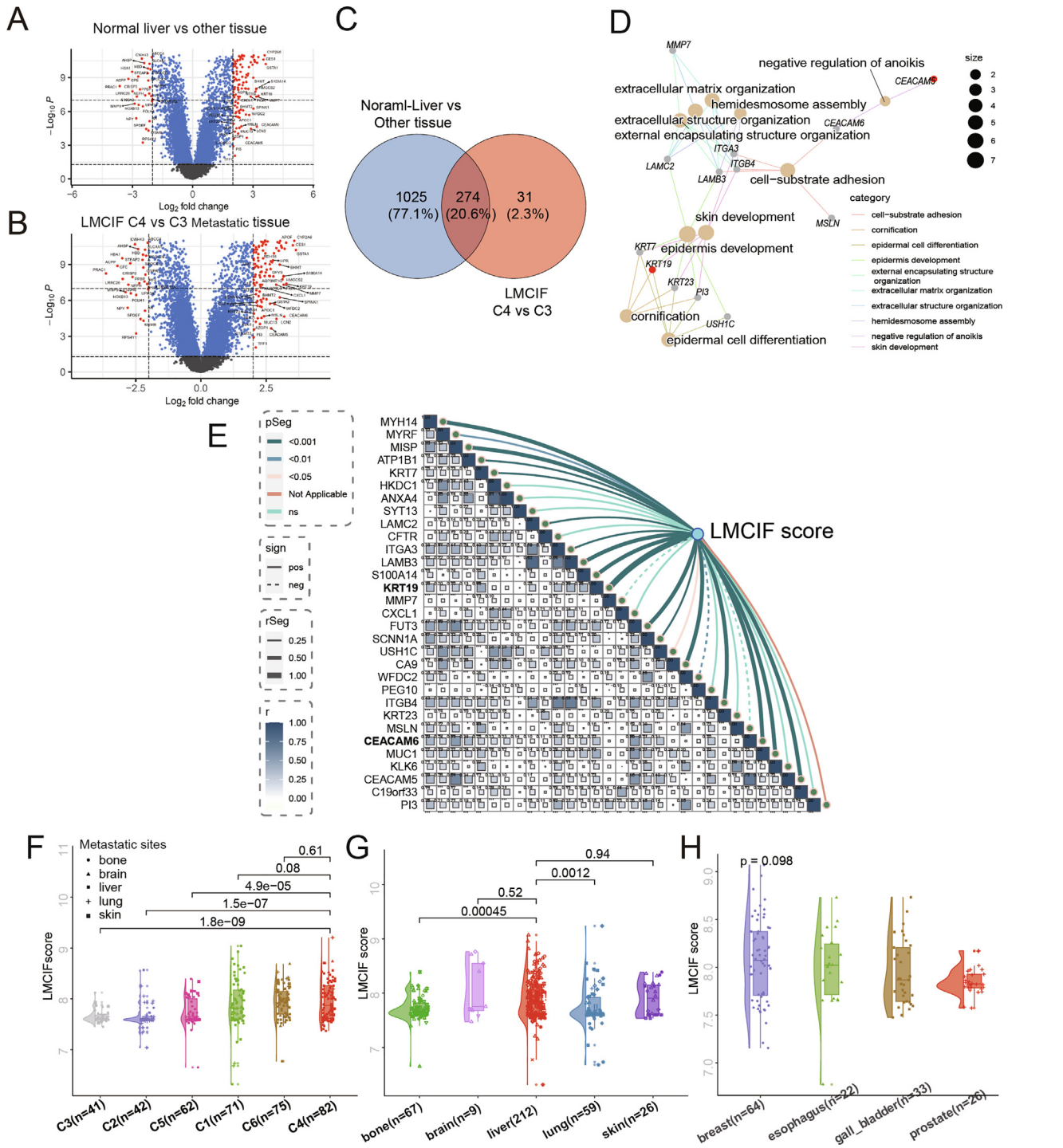

Fig. 5. Development of LMCIF score in metastasis patients. A) Volcano plot of limma analysis for DEGs between normal liver and other normal tissue. B) Volcano plot of DEGs between liver metastasis and other organ metastases. C) Venn plot for the cross selection of the special DEGs of LMCIF C4 cluster and normal liver samples. D) GO terms Functional analysis of 31 DEGs of LMCIF clusters. E) Spearman correlation analysis of LMCIF score with 31 DEGs. F) Wilcoxon test for the different expressions of LMCIF score in LMCIF clusters. G) Wilcoxon test for the different expressions of LMCIF score in different organ metastasis tissues. F) Kruskal-Wallis test for the expression of LMCIF score in different cancer types.

experiments were performed based on 25 samples from 4 pan-cancer metastasis, including liver (n = 16), bone (n = 4), brain (n = 2) and lung (n = 3), for KRT19 (CK19) and CD8 protein. Here, three representative samples with different expression modes of KRT19 and CD8 were selected to show the features of LMCIF in pan-cancer(Fig. 7**B, 7C and 7D**). Fig. 7**B** showed one representative sample with low KRT 19 and high CD8 expression in LM samples, and Fig. 7**C** showed the representative sample with high KRT19 and low CD8 expression in LM samples. As a compared group, 2/3 of lung metastasis had high CD8 expression and low KRT19 and a sample with high CD8 was selected as the representative sample (Fig. 7**D**). The expression mode of KRT19 and CD8 is shown in Fig. 7**E**. Interestingly, 4 of 16 LM samples with high KRT19 and low CD8 could be represented as LMCIF clusters. Among 16 LM

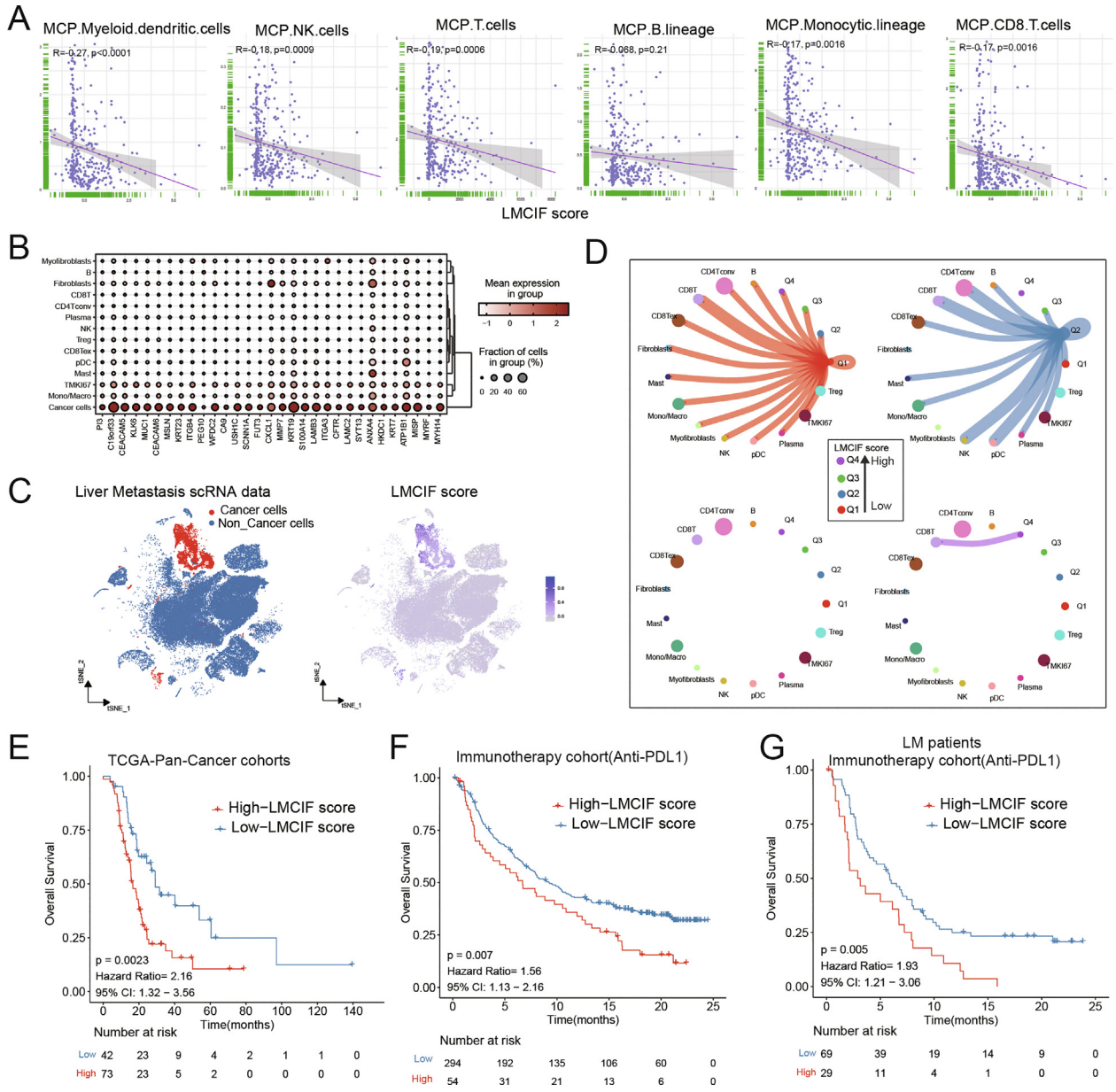

Fig. 6. Immunological and prognostic features of LMCIF score. A) Spearman correlation analysis of LMCIF score with immune cells in LM patients(n = 212). B) Expression of LMCIF in each type at single-cell level in LM patients with scRNA data. C) The tSNE plot of LMCIF score in the scRNA data of cancer cells and non-cancer cells. D) Cell communication analysis results of LMCIF groups in LM single cells. E) Log-rank test for LMCIF score in LM patients without Immunotherapy(n = 115). F) Log-rank test for LMCIF score in a cohort with immunotherapy(n = 348). G) Log-rank test for LMCIF score in LM patients with Immunotherapy(n = 98).

samples, it was revealed that KRT19 was negatively related to CD8 (Fig. 7**F**). An additional set of 79 samples with LM from CRC cancer were extracted to further validate the complex correlation of LMCIFgenes with immune cells (Supplemental **Figure S7**) and the negative correlation between KRT19 and CD8 (Fig. 7**G**). Finally, we calculated the relationship between KRT19 and lymphocyte cells based on EstimateScore in the 79 LM samples, and we found that KRT19 was significantly negatively related to CD8 T cells, immune score, stromal score and estimate score (Fig. 7**H**), partially validating the immunosuppression environment was associated with KRT19.

The hypothesis of microenvironment identification of liver metastasis

In summary, a hypothesis for LMCIF across cancer types was proposed to characterize the features of LM (Fig. 8). Among LM samples, the cluster with the highest LM was termed the LMCIF cluster, which showed an extreme immune-desert phenotype, thus giving us novel insights at the clinical level. Accordingly, the LMCIF score was developed to better understand the TME of LM. Along with their high expression of LMCIF score, LM samples tended to be less immunogenic, while samples with low LMCIF score tended to be more immunogenic. Therefore, we further speculated that the LMCIF score could be used as a predictor of immunotherapy response.

Discussion

To the best of our knowledge, the current study, for the first time, attempts a systematic study of immunological features of LM by combining clinical data and RNA omics in metastasis samples across several cancer types. Using bioinformatics, the multi-

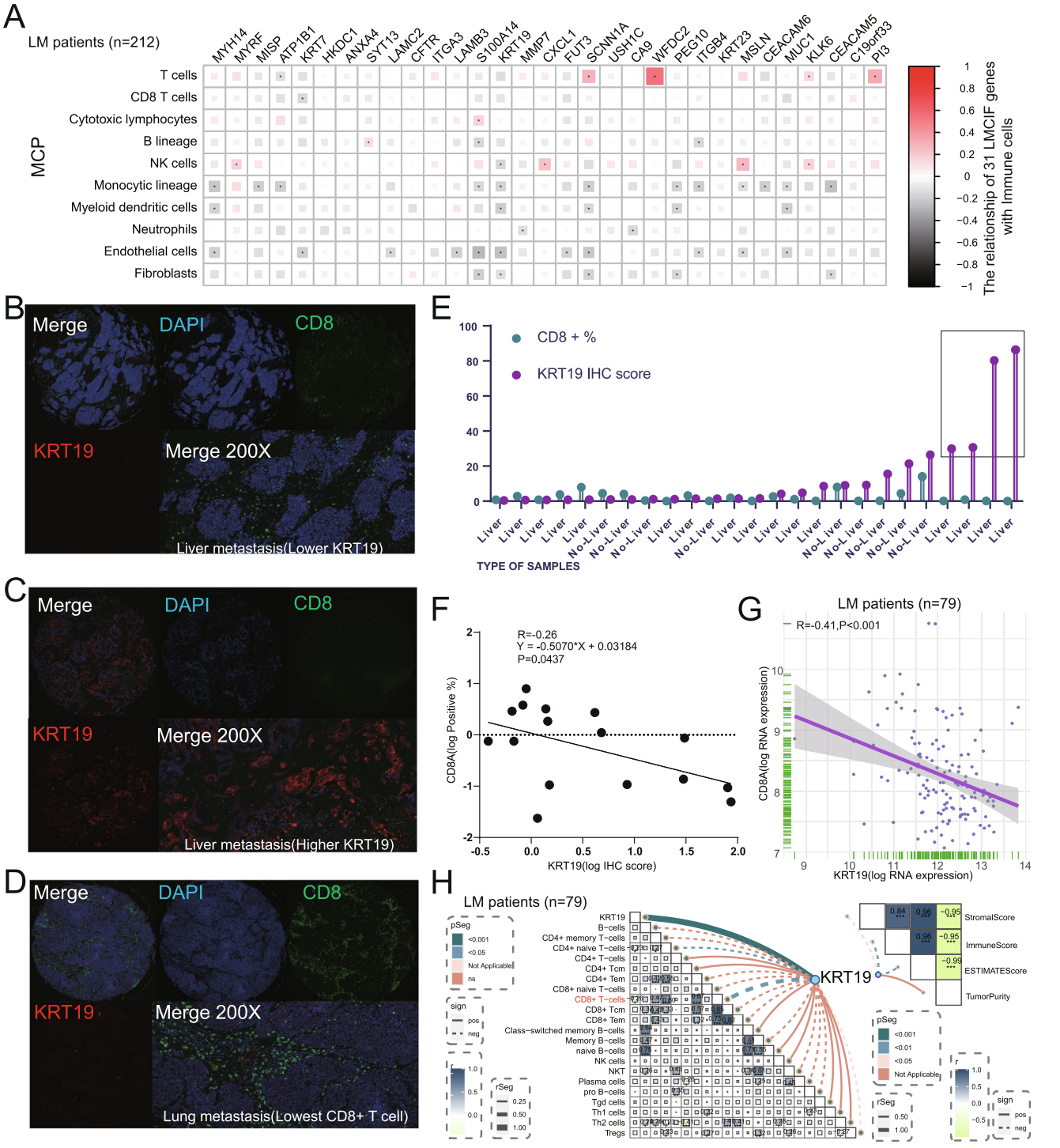

Fig. 7. Validation of the LMCIF score in in-house and external cohorts. A) Spearman correlation of 31 LMCIF genes with MCP TME cells in the LM patients(n = 212). B) IHC for the representative LM sample with both low CD8 and KRT19 expression. C) IHC for the representative LM sample with no CD8 expression and extremely high KRT19 expression. D) IHC for the representative lung metastasis sample with high CD8 and low KRT19 expression. E) Dot plot for the rank of CD8 and KRT19 in 25 IHC samples. F) Linear regression analysis of CD8 and KRT19 protein expression in 16 LM samples by IHC. G) Spearman correlation of CD8 and KRT19 RNA gene expression in the GSE51244 (n = 79). H) Spearman correlation of KRT19 with immune features and TME cells in the GSE51244(n = 79).

omics immunosuppressive features of the LMCIF cluster were further explored. In addition, regardless of an organ's initial cancer location, LM patients showed more immunosuppressive TME than those with other organ metastases.

LM is one of the most common secondary sites invaded by disseminated tumor cells and tends to have a worse prognosis than patients with metastasis in other organs, as studied in>10,000 metastasis patients. To investigate the TME of LM, 373 metastasis samples, including liver, lung, brain, bone, and skin metastasis from>16 cancer types, were collected in this study. It was noted that patients with LM had lower TMB, which is an independent biomarker positively associated with the response rate to immune checkpoint blockade therapy[29]. In agreement, the infiltration of various immune cells was less in patients with LM than in those

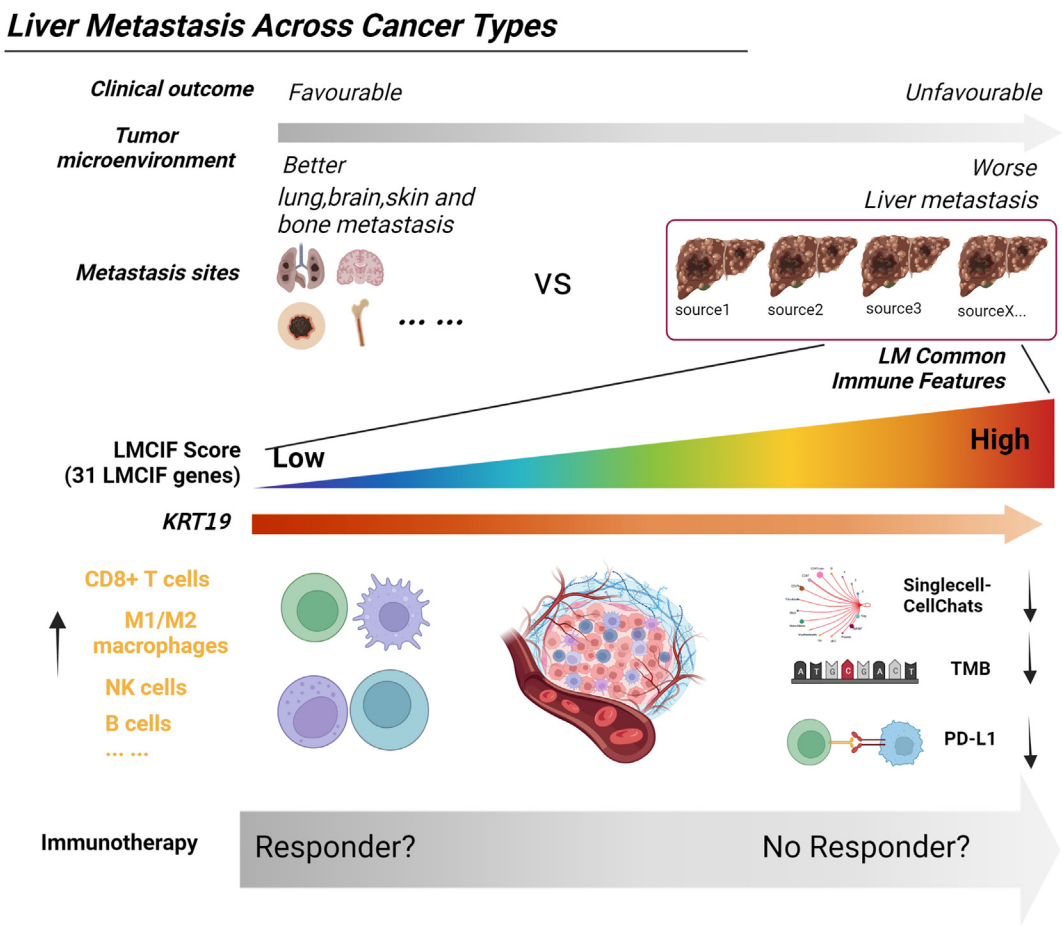

Fig. 8. Hypothesis of LMCIF. Based on LM co-expression immune pathways, metastatic samples could be divided into six immune-related clusters. A higher LMCIF score tends to be less immunogenic, while a lower LMCIF score tends to be more immunogenic. LMCIF genes, including KRT19, might be accorded the same function as the LMCIF score. Patients with low LMCIF scores might have better immunotherapy responses and prognoses.

without LM metastasis. Importantly, these results were further validated by IHC, showing a significantly lower infiltration of $CD8^+$ T cells in LM tumor tissue compared with those in non-LM tumor metastasis. These discoveries were consistent with the results based on multiple mouse models showing that liver metastases can hijack immunological tolerance mechanisms of the liver to induce systemic tumor-specific CD8 + T cell loss and cause impaired immunity[16]. Notably, we, for the first time, validated this phenomenon based on a large cohort of LM patients, suggesting that liver metastases may play a significant role in determining immunotherapy success.

Moreover, a cross-selection was conducted to identify the 29 LMSIPs from MSigDB. Metastasis samples were clustered according to the GSVA score of 29 LMSIPs, and the one of these clusters with the highest proportion of LM was detected, both in Dan R. Robinson et al.[18] and Sandra García-Mulero et al.[30] cohorts. In line with previous results, the LMCIF cluster showed a higher LM percentage, and lymphoid and myeloid cell lineages in this cluster were significantly reduced. In addition, some stromal cells were highly expressed in the LMCIF cluster. It has been reported that liver stromal cells can suppress immunity by stimulating non-responsive cells, as well as myeloid-derived suppressor cells (MDSCs), thereby compromising the performance of antigen-presenting cells [31]. Combined with our results, it can be inferred that the immune suppressive influence of liver metastases on TME is not only derived from the inhibition of tumor cytotoxic $CD8^+$ T cells, but also through the induction of stromal cells.

To facilitate clinical usage of the signature of LMCIF cluster, 31 DEGs were obtained to develop an LMCIF score for simplifying the features of the LMCIF cluster. The prognostic and predictive value of the LMCIF score implies its potential in clinical practice. In addition, cell analysis showed that 31 LMCIF genes and LMCIF score were specifically expressed in tumor cells, not in immune cells, indicating that the LMCIF score is a good representation of tumor states. Additional analysis revealed that these 31 DEGs were closely associated with cell-substrate adhesion. The adhesion of circulating cancer cells is the initial step, and it has a decisive role in the formation of liver metastases[32]. It was also demonstrated that metastases in the liver showed a higher LMCIF score than metastases in bone and lung. Of note, no differences were found in the LMCIF score, regardless of their primary sites: breast, esophagus gallbladder, and prostate cancer. This implies that different cancer-derived metastases might share a common mechanism for immune tolerance to the liver.

Further analysis revealed a strong negative association between LMCIF score and several immune cells involved in both innate and adaptive immune responses, such as $CD8^+$ T cells, myeloid cells, dendritic cells, NK cells, and B cells. This further supports our results that liver metastases might cultivate an immune-desert phenotype and it might diminish immunity systemically. Furthermore, intercellular communication networks were analyzed based on single-cell data and also illustrated that a higher LMCIF immune score would result in impairing communication among these immune cells. This indicates that liver metastases have a detrimen-

tal impact on immune cell communication quality in addition to their negative impact on immune cell quantity. We also discovered a lot of negative correlations between 31 LMCIF genes and TME cells in the patients with LM. Among these genes, keratin 19 (KRT19) was found to have a strong positive correlation with the LMCIF immune score. Additionally, it was negatively associated with CD8 + T cells, which was confirmed through immunohistochemistry (IHC). As a small type I cytokeratin, KRT19 is a poor prognostic marker for liver cancer and other tumors [33–34]. A recent mouse *in vivo* study further revealed that KRT19 contributes to the absence of activated intertumoral T cells, and compromises the effectiveness of anti-PD-1 immunotherapy[35]. Moreover, as required for cell proliferation, KRT19 was also suggested to be used to predict the efficacy of cyclin-dependent kinase inhibitors for treatments of breast cancer[36]. In addition to the discovery of KRT19, several other genes in LMCIF, including the novel immune checkpoints(CEACAM5[37] and CEACAM6[38–39]), have been found to possess significant immunosuppressive effects.The discovery of these vital molecules involved in immune response further verifies the reliability of LMCIF score. Thus, by conducting further investigations into other LMCIF genes, we may uncover novel targets that could enhance the effectiveness of immunotherapy. Furthermore, conducting future research focused on elucidating a pattern that connects either all or a subset of the elements within the 31-gene signature holds great importance for advancing studies on the immunobiology of liver metastases and cancer in a broader sense.

Conclusions

In conclusion, our results suggest that liver metastases from different primary cancers may share similar immunological profiles that induce immune tolerance and escape from immune monitoring, regardless of the primary sites. LM immune-related cluster was utilized to establish an LMCIF immune score for predicting the prognosis and immunotherapy response of LM patients, which might benefit clinical disease management.

Funding

This work was supported by the Natural Science Foundation of China (No: 81972012), Key Research and Development Program of Zhejiang Province (2021C03056) and the Natural Science Foundation of Zhejiang Province (LQ21H200004).

Data availability statement

The datasets used and/or analyzed during the current study are available in the public domain. All R scripts are aviable in the Github(https://github.com/YzGLab/LMimmune) and other custom scripts for analyzing data are available upon reasonable request.

Ethics statement

The use of all human samples were approved by the Institutional Ethics Committee of the Sir Run Run Shaw Hospital of Zhejiang University School of Medicine (Ethical code: 20190211-55). Informed consent was obtained from all patients.

Declaration of Competing Interest

The authors declare that they have no known competing financial interests or personal relationships that could have appeared to influence the work reported in this paper.

Appendix A. Supplementary data

Supplementary data to this article can be found online at https://doi.org/10.1016/j.jare.2023.08.011.

References

[1] Milette S, Sicklick JK, Lowy AM, Brodt P. Molecular Pathways: Targeting the Microenvironment of Liver Metastases. Clin Cancer Res 2017;23(21):6390–639.
[2] Li X, Ramadori P, Pfister D, Seehawer M, Zender L, Heikenwalder M. The immunological and metabolic landscape in primary and metastatic liver cancer. Nat Rev Cancer 2021;21(9):541–57.
[3] Siegel RL, Miller KD, Jemal A. Cancer statistics, 2020. CA: a cancer journal for clinicians 2020;**70**(1):7-30.
[4] Llovet JM, Ricci S, Mazzaferro V, Hilgard P, Gane E, Blanc JF, et al. Sorafenib in advanced hepatocellular carcinoma. N Engl J Med 2008;359(4):378–90.
[5] Llovet JM, Montal R, Villanueva A. Randomized trials and endpoints in advanced HCC: Role of PFS as a surrogate of survival. J Hepatol 2019;70(6):1262–77.
[6] Abou-Alfa GK, Meyer T, Cheng AL, El-Khoueiry AB, Rimassa L, Ryoo BY, et al. Cabozantinib in Patients with Advanced and Progressing Hepatocellular Carcinoma. N Engl J Med 2018;379(1):54–63.
[7] Keenan BP, Fong L, Kelley RK. Immunotherapy in hepatocellular carcinoma: the complex interface between inflammation, fibrosis, and the immune response. J Immunother Cancer 2019;7(1):267.
[8] Mizukoshi E, Kaneko S. Immune cell therapy for hepatocellular carcinoma. J Hematol Oncol 2019;12(1):52.
[9] Knolle PA, Thimme R. Hepatic immune regulation and its involvement in viral hepatitis infection. Gastroenterology 2014;146(5):1193–207.
[10] Heymann F, Peusquens J, Ludwig-Portugall I, Kohlhepp M, Ergen C, Niemietz P, et al. Liver inflammation abrogates immunological tolerance induced by Kupffer cells. Hepatology 2015;62(1):279–91.
[11] Jenne CN, Kubes P. Immune surveillance by the liver. Nat Immunol 2013;14(10):996–1006.
[12] Curiel TJ. Tregs and rethinking cancer immunotherapy. J Clin Invest 2007;117(5):1167–74.
[13] Ringelhan M, Pfister D, O'Connor T, Pikarsky E, Heikenwalder M. The immunology of hepatocellular carcinoma. Nat Immunol 2018;19(3):222–32.
[14] Pacella I, Procaccini C, Focaccetti C, Miacci S, Timperi E, Faicchia D, et al. Fatty acid metabolism complements glycolysis in the selective regulatory T cell expansion during tumor growth. PNAS 2018;115(28):E6546–55.
[15] Thomson AW, Vionnet J, Sanchez-Fueyo A. Understanding, predicting and achieving liver transplant tolerance: from bench to bedside. Nat Rev Gastroenterol Hepatol 2020;17(12):719–39.
[16] Yu J, Green MD, Li S, Sun Y, Journey SN, Choi JE, et al. Liver metastasis restrains immunotherapy efficacy via macrophage-mediated T cell elimination. Nat Med 2021;**27**(1):152-64.
[17] Nguyen B, Fong C, Luthra A, Smith SA, DiNatale RG, Nandakumar S, et al. Genomic characterization of metastatic patterns from prospective clinical sequencing of 25,000 patients. Cell 2022;185(3):563–75 e11.
[18] Robinson DR, Wu YM, Lonigro RJ, Vats P, Cobain E, Everett J, et al. Integrative clinical genomics of metastatic cancer. Nature 2017;548(7667):297–303.
[19] Mariathasan S, Turley SJ, Nickles D, Castiglioni A, Yuen K, Wang Y, et al. TGFbeta attenuates tumour response to PD-L1 blockade by contributing to exclusion of T cells. Nature 2018;554(7693):544–58.
[20] Sinha N, Sinha S, Valero C, Schaffer AA, Aldape K, Litchfield K, et al. Immune Determinants of the Association between Tumor Mutational Burden and Immunotherapy Response across Cancer Types. Cancer Res 2022;82(11):2076–83.
[21] Che LH, Liu JW, Huo JP, Luo R, Xu RM, He C, et al. A single-cell atlas of liver metastases of colorectal cancer reveals reprogramming of the tumor microenvironment in response to preoperative chemotherapy. Cell Discovery 2021;7(1):80.
[22] Aran D, Hu Z, Butte AJ. xCell: digitally portraying the tissue cellular heterogeneity landscape. Genome Biol 2017;18(1):220.
[23] Chen S, Gao Y, Wang Y, Daemen T. The Combined Signatures of Hypoxia and Cellular Landscape Provides a Prognostic and Therapeutic Biomarker in HBV-Related Hepatocellular Carcinoma. Int J Cancer 2022. doi: https://doi.org/10.1002/ijc.34045.
[24] Becht E, Giraldo NA, Lacroix L, Buttard B, Elarouci N, Petitprez F, et al. Estimating the population abundance of tissue-infiltrating immune and stromal cell populations using gene expression. Genome Biol 2016;17(1):218.
[25] Gao Y, Chen S, Vafaei S, Zhong X. Tumor-Infiltrating Immune Cell Signature Predicts the Prognosis and Chemosensitivity of Patients With Pancreatic Ductal Adenocarcinoma. Front Oncol 2020;10:557638.
[26] Yoshihara K, Shahmoradgoli M, Martinez E, Vegesna R, Kim H, Torres-Garcia W, et al. Inferring tumour purity and stromal and immune cell admixture from expression data. Nat Commun 2013;4:2612.
[27] Gao Y, Wang H, Li H, Ye X, Xia Y, Yuan S, et al. Integrated analyses of m(1)A regulator-mediated modification patterns in tumor microenvironment-infiltrating immune cells in colon cancer. Oncoimmunology 2021;10(1):1936758.

[28] Budwit-Novotny DA, McCarty KS, Cox EB, Soper JT, Mutch DG, Creasman WT, et al. Immunohistochemical analyses of estrogen receptor in endometrial adenocarcinoma using a monoclonal antibody. Cancer Res 1986;46 (10):5419–25.
[29] Klempner SJ, Fabrizio D, Bane S, Reinhart M, Peoples T, Ali SM, et al. Tumor Mutational Burden as a Predictive Biomarker for Response to Immune Checkpoint Inhibitors: A Review of Current Evidence. Oncologist 2020;25(1): e147–59.
[30] Garcia-Mulero S, Alonso MH, Pardo J, Santos C, Sanjuan X, Salazar R, et al. Lung metastases share common immune features regardless of primary tumor origin. J Immunotherapy Cancer 2020;**8**(1).
[31] Schildberg FA, Sharpe AH, Turley SJ. Hepatic immune regulation by stromal cells. Curr Opin Immunol 2015;32:1–6.
[32] Izutsu R, Osaki M, Jehung JP, Seong HK, Okada F. Liver Metastasis Formation Is Defined by AMIGO2 Expression via Adhesion to Hepatic Endothelial Cells in Human Gastric and Colorectal Cancer Cells. Pathol Res Pract 2022;237:154015.
[33] Rhee H, Kim HY, Choi JH, Woo HG, Yoo JE, Nahm JH, et al. Keratin 19 Expression in Hepatocellular Carcinoma Is Regulated by Fibroblast-Derived HGF via a MET-ERK1/2-AP1 and SP1 Axis. Cancer Res 2018;78(7):1619–31.
[34] Menz A, Bauer R, Kluth M, Marie von Bargen C, Gorbokon N, Viehweger F, et al. Diagnostic and prognostic impact of cytokeratin 19 expression analysis in human tumors: a tissue microarray study of 13,172 tumors. Hum Pathol 2021;115:19–36.
[35] Wang Z, Moresco P, Yan R, Li J, Gao Y, Biasci D, et al. Carcinomas assemble a filamentous CXCL12-keratin-19 coating that suppresses T cell-mediated immune attack. Proc Natl Acad Sci U S A 2022;**119**(4):e2119463119.
[36] Sharma P, Alsharif S, Bursch K, Parvathaneni S, Anastasakis DG, Chahine J, et al. Keratin 19 regulates cell cycle pathway and sensitivity of breast cancer cells to CDK inhibitors. Sci Rep 2019;9(1):14650.
[37] Teijeira A, Migueliz I, Garasa S, Karanikas V, Luri C, Cirella A, et al. Three-dimensional colon cancer organoids model the response to CEA-CD3 T-cell engagers. Theranostics 2022;12(3):1373–87.
[38] Pinkert J, Boehm HH, Trautwein M, Doecke WD, Wessel F, Ge Y, et al. T cell-mediated elimination of cancer cells by blocking CEACAM6-CEACAM1 interaction. Oncoimmunology 2022;11(1):2008110.
[39] Huang YH, Zhu C, Kondo Y, Anderson AC, Gandhi A, Russell A, et al. CEACAM1 regulates TIM-3-mediated tolerance and exhaustion. Nature 2015;517 (7534):386–90.